PHYSICAL REVIEW C VOLUME 10, NUMBER 6 DECEMBER 1974

Renormalized Brueckner-Hartree-Fock and density dependent Hartree-Fock theories of finite nuclei*

K. T. R. Davies†
Los Alamos Scientific Laboratory, University of California, Los Alamos, New Mexico 87544 and Oak Ridge National Laboratory, Oak Ridge, Tennessee 37830

R. J. McCarthy
University of Arizona, Tucson, Arizona 85721

J. W. Negele‡ and P. U. Sauer§
Los Alamos Scientific Laboratory, University of California, Los Alamos, New Mexico 87544 and Laboratory for Nuclear Science and Department of Physics, Massachusetts Institute of Technology, Cambridge, Massachusetts 02139

(Received 4 September 1974)

Renormalized Brueckner-Hartree-Fock and density dependent Hartree-Fock calculations in the literature have been difficult to compare because they involve both different physical approximations and also technical computational differences. Hence, results obtained in both calculations for ^{40}Ca are corrected for technical differences and compared in detail. It is shown that comparable Brueckner-Hartree-Fock calculations using an oscillator basis and using the local density approximation are in good numerical agreement, and that three mechanisms are of roughly equal importance in obtaining the proper interior density: occupation probabilities, the potential arising from the variation of the Pauli operator, and the phenomenological parametrization of higher order corrections to the effective nuclear interaction. The renormalized oscillator basis calculations include only the effect of occupation probability diagrams. The "bare" local density approximation results are an improvement over the renormalized results since the former includes the effects of both occupation probabilities and the variation of the Pauli operator. The adjusted local density approximation calculations then give further improvement due to the phenomenological parametrization of the force, simulating the effect of higher-order diagrams.

[NUCLEAR STRUCTURE Renormalized Brueckner-Hartree-Fock and density dependent Hartree-Fock theory. Application to ^{40}Ca.]

I. INTRODUCTION

Renormalized Brueckner-Hartree-Fock (RBHF) and density dependent Hartree-Fock (DDHF) calculations of the ground states of finite nuclei differ both in the physical content of the theory and in technical computational details. Hence, it is desirable for the present authors who have been involved in both types of calculations[1-3] to account for the technical differences and to display the contributions to ground state observables arising from the different physical content of the theories. The nucleus ^{40}Ca was selected for this comparison because the most complete computational results required for this comparison were already available in the literature. Although no new computational results are presented in this note, it is hoped that the present comments will be of some pedagogical value in clarifying the relationship of these two types of calculations.

RBHF is the most fundamental attempt to numerically evaluate self-consistent wave functions in the basis defined diagrammatically by graphs (a) and (b) of Fig. 1, with a minimum of additional simplifying approximations.[1,2] The wave functions are expanded in an oscillator basis. In the reaction matrix G, the main approximation is to replace the Pauli projection operator Q by the "angle averaged" Q for pure oscillator wave functions with a predetermined value of $\hbar\Omega$. For ^{40}Ca, the oscillator approximation of Q is reasonably accurate and $\hbar\Omega = 12.5$ MeV corresponds to a density distribution close to the calculated result, so that this approximation is expected to be quite satisfactory.

DDHF is based on G matrices with purely kinetic intermediate states, as is the BHF with which we compare. Nevertheless, DDHF differs from BHF in three significant respects[3]: (1) the local density approximation (LDA) is used; (2) the single particle potential is defined variationally; and (3) the effects of omitted diagrams and relativistic and

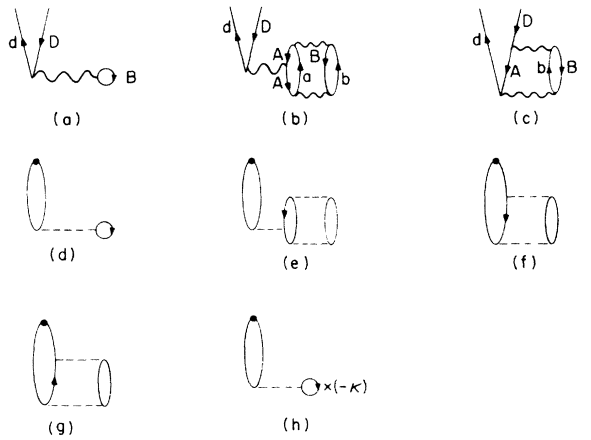

FIG. 1. (a)–(c) Diagrams for the single-particel potential and (d)–(h) for the expansion of the one-body density operator. The wavy lines indicate G and the dashed lines denote V.

mesonic corrections are approximated phenomenologically.

In the propagator $Q[H_0 - W]^{-1}Q$ of the reaction matrix with $H_0 = QTQ$, the local density approximation replaces the exact global Pauli projector Q for the finite nucleus by the nuclear matter Pauli projector $Q_{\rm NM}$ corresponding to the density at the center of mass of the two interacting particles. Although $Q_{\rm NM}$ certainly does not approximate Q globally, the propagator only contributes within the range of the two body force, and locally at small relative distances Q is well approximated by $Q_{\rm NM}$. This may be seen simply in coordinate space by writing

$$\langle \vec{x}\vec{y} \mid Q \mid \vec{x}'\vec{y}' \rangle = [\delta(\vec{x}-\vec{x}') - \rho(\vec{x},\vec{x}')][\delta(\vec{y}-\vec{y}') - \rho(\vec{y},\vec{y}')]$$

and comparing the exact density matrix for neutrons or protons $\rho(\vec{R}+\frac{1}{2}\vec{r}, \vec{R}-\frac{1}{2}\vec{r})$ in cm and relative coordinates, $\vec{R}$ and $\vec{r}$, respectively, with the nuclear matter density matrix $\rho(R)[3j_1(k_f r)/k_f r]$ as in Ref. 4 where $k_f = [3\pi^2\rho(R)]^{1/3}$. The accuracy of the LDA in ^{40}Ca will be verified below in Sec. II.

The variational definition of the single particle potential has been a subject of considerable interest.[5-8] For our present purposes, we shall not attempt to justify it, but rather show that the variation of an appropriate expression yields the diagrams (a) through (c) of Fig. 1. We define

$$\langle H \rangle = \sum_A \langle A \mid T \mid A \rangle + \frac{1}{2}\sum_{AB} \langle AB \mid G(\epsilon_A + \epsilon_B) \mid AB \rangle , \tag{1}$$

where $\langle AB \mid G(\epsilon_A + \epsilon_B) \mid AB \rangle$ is assumed to be antisymmetrized and

$$\epsilon_A = T_A + \sum_B \langle AB \mid G(\epsilon_A + \epsilon_B) \mid AB \rangle .$$

Occupied and unoccupied states are denoted by upper case and lower case roman letters, respectively. Instead of performing an unrestricted variation using Lagrange multipliers, it is preferable to define the self-consistent single particle state by requiring stationarity with respect to an arbitrary infinitesimal unitary transformation between the occupied and unoccupied state wave functions. Writing:

$$\begin{aligned} \mid D' \rangle &= \mid D \rangle + \lambda \mid d \rangle \\ \mid d' \rangle &= \mid d \rangle - \lambda^* \mid D \rangle , \end{aligned} \tag{2}$$

requiring stationarity for any D and d, and collecting the terms associated with λ^* yields

$$\delta(H) = \lambda^* \Big\{ \langle d \mid T \mid D \rangle + \sum_B \langle dB \mid G(\epsilon_D + \epsilon_B) \mid DB \rangle + \sum_{\substack{AB \\ b}} \langle AB \mid G(\epsilon_A + \epsilon_B) \mid Db \rangle \langle db \mid \frac{1}{H_0 - \epsilon_A - \epsilon_B} \mid db \rangle \langle db \mid G(\epsilon_A + \epsilon_B) \mid AB \rangle \Big\}$$

$$- \frac{1}{2}\sum_{\substack{AB \\ ab}} \langle AB \mid G(\epsilon_A + \epsilon_B) \mid ab \rangle \langle ab \mid \frac{1}{(H_0 - \epsilon_A - \epsilon_B)^2} \mid ab \rangle \langle ab \mid G(\epsilon_A + \epsilon_B) \mid AB \rangle (\delta\epsilon_A + \delta\epsilon_B) . \tag{3}$$

Variation of ϵ_A is similar, with the result

$$\delta\epsilon_A = \lambda^* \Big\{ \delta_{AD} \Big[\langle d \mid T \mid D \rangle + \sum_C \langle dC \mid G(\epsilon_D + \epsilon_C) \mid DC \rangle \Big] + \langle dA \mid G(\epsilon_A + \epsilon_D) \mid DA \rangle$$

$$+ 2\sum_{Cb} \langle AC \mid G(\epsilon_A + \epsilon_C) \mid Db \rangle \langle db \mid \frac{1}{H_0 - \epsilon_A - \epsilon_C} \mid db \rangle \langle db \mid G(\epsilon_A + \epsilon_C) \mid AC \rangle \Big\}$$

$$- \sum_{\substack{C \\ ab}} \langle AC \mid G(\epsilon_A + \epsilon_C) \mid ab \rangle \langle ab \mid \frac{1}{(H_0 - \epsilon_A - \epsilon_C)^2} \mid ab \rangle \langle ab \mid G(\epsilon_A + \epsilon_C) \mid AC \rangle (\delta\epsilon_A + \delta\epsilon_C) . \tag{4}$$

No corresponding variation for the particle energies arises, since we have defined H_0 to be QTQ.

Equation (4) is a set of linear equations which may be solved exactly by matrix inversion. The leading term is

$$\delta\epsilon_A = \lambda^* \langle dA \mid G(\epsilon_A + \epsilon_D) \mid DA \rangle + \cdots , \tag{5}$$

since according to Eq. (3) with the condition $\delta(H) = 0$, the first term in Eq. (4) is of higher order in G. To obtain the lowest order diagrams defining the potential U, it is sufficient to retain this leading term, to substitute $\delta\epsilon_A + \delta\epsilon_B$ in Eq. (3), to note that $\delta\epsilon_A$ and $\delta\epsilon_B$ yield equal contributions, and define $\langle d \mid U \mid D \rangle$ by the relation $\delta\langle H \rangle = \lambda^* \{ \langle d \mid T \mid D \rangle + \langle d \mid U \mid D \rangle \}$ which assures stationarity. Hence,

$$\langle d \mid U \mid D \rangle = \sum_B \langle dB \mid G(\epsilon_D + \epsilon_B) \mid DB \rangle + \sum_{ABb} \langle AB \mid G(\epsilon_A + \epsilon_B) \mid Db \rangle \frac{1}{\epsilon_b + \epsilon_d - \epsilon_A - \epsilon_B} \langle db \mid G(\epsilon_A + \epsilon_B) \mid AB \rangle$$

$$- \sum_{\substack{AB \\ ab}} \langle AB \mid G(\epsilon_A + \epsilon_B) \mid ab \rangle \frac{1}{(\epsilon_a + \epsilon_b - \epsilon_A - \epsilon_B)^2} \langle ab \mid G(\epsilon_A + \epsilon_B) \mid AB \rangle \langle dA \mid G(\epsilon_A + \epsilon_D) \mid DA \rangle . \tag{6}$$

The three terms in Eq. (6) correspond to diagrams (a), (c), and (b) in Fig. 1, respectively, where the propagator in this figure are labeled appropriately. Note that all G matrices are evaluated on energy shell, corresponding to a sum of diagrams over relative time orderings and that the minus sign associated with diagram (b) is consistent with the three hole lines and two closed loops. Also, it is important to note that diagram (c) exactly represents the variation of the Pauli operator, whereas the occupation probability diagram (b) represents only the leading term of an infinite series solution to Eq. (4).

Thus, we conclude that stationarity of Eq. (1) is equivalent to the diagramatic definitions of the particle-hole single particle potential specified by graphs (a) through (c) of Figure 1. The DDHF single-particle potential, while not rigorously identical, very closely approximates these graphs, since it is defined by the stationarity of Eq. (1) with Q replaced by Q_{NM}, and this local density approximation has already been shown above to be extremely accurate.

The final approximation in DDHF is to represent the additional many-body, relativistic, and mesonic corrections by a zero range phenomenological interaction in the triplet even states, where nuclear matter estimates indicate such corrections to be largest. These effects roughly account for the discrepancy of 5 MeV per particle between the two-body cluster energy of 11 MeV per particle in nuclear matter and the binding energy extrapolated from the semiempirical mass formula, and are thus necessary to reproduce the observed binding energies and single-particle energies of finite nuclei. In addition to increasing the binding energy, this phenomenological correction term is adjusted to saturate nuclear matter at $k_F = 1.34$ fm^{-1} to obtain the observed nuclear charge radii.

To avoid confusion in terminology, one should note that Campi and Sprung[9] refer to this correction term as a renormalization, which is unrelated to the renormalization in RBHF associated with the inclusion of diagram (b) of Fig. 1 in the definition of the single-particle potential.

II. COMPARISON OF DDHF AND RBHF

From the preceding discussion, it is evident that DDHF and RBHF differ in several respects. RBHF includes only diagrams (a) and (b) of Fig. 1 in the definition of the single-particle potential. DDHF also contains diagram (c) and in addition includes the parametrization of higher order corrections and utilizes the LDA. In this section, we shall attempt to separate the effects of diagrams (a), (b), and (c) of Fig. 1 and the parametrization of higher order corrections in ^{40}Ca using the published results of Refs. 1–3, and check the accuracy of the LDA in technically comparable calculations.

It will be convenient to distinguish the following five calculations of ^{40}Ca which are all based on reaction matrices with purely kinetic energies in intermediate states: (1) BHF, the unrenormalized Brueckner-Hartree-Fock calculation of Table IV of Ref. 2 using QTQ as the single-particle Hamiltonian for intermediate states; (2) LDAHF, the Hartree-Fock calculation denoted HF-bare in Table VII and graphed in Fig. 4 of Ref. 3, using the local density approximation with the bare Reid potential omitting all $\delta G/\delta\rho$ terms; (3) RBHF, the renormalized Brueckner-Hartree-Fock calculation of Table IV and Fig. 3 of Ref. 2; (4) DDHF, the density dependent Hartree-Fock calculation with the bare Reid potential of Table VII and Fig. 4 of Ref. 3 and; 5) adjusted DDHF, the density dependent Hartree-Fock calculation including a phenomenological parametrization of higher order corrections, of Table VII and Fig. 4 of Ref. 3.

In order to compare the local density approxima-

tion results from Ref. 3 with the oscillator basis results of Refs. 1 and 2, it is necessary to correct for several technical differences in the calculations. For readers uninterested in technical considerations, it is sufficient to regard BHF and LDAHF as identical, assume that the results in Fig. 2 result from technically comparable calculations, and go on to the next section. For those interested in a detailed comparison of the two approaches, we show below how to approximately correct for the technical differences directly from the published results of Refs. 1, 2, and 3.

The validity of the local density approximation may be verified by comparing the energies and densities obtained in the BHF and LDAHF calculations. The LDAHF binding energy per particle of 3.0 MeV appears superficially to disagree significantly from the BHF result of 3.9 MeV. However, this difference of 0.9 MeV may be roughly accounted for by three technical differences in the two calculations, namely, (i) the different treatment of the available energy for interacting protons, (ii) inclusion of different partial waves of the nuclear force, and (iii) different treatment of the exchange Coulomb contribution.

(i) Whereas in principle, the Coulomb contribution to the single particle energy should appear in both occupied and unoccupied proton states, in practice, the Coulomb potential is always omitted from the unoccupied state spectrum. Hence, as argued in Ref. 3, the most consistent approximation is to also explicitly subtract off the Coulomb energy from the occupied state single-particle energies, which is correct to the extent to which excited and unexcited protons see the same Coulomb potential. The BHF calculations do not remove the Coulomb energy, so the occupied state spectrum is shifted upward by an average Coulomb energy of 7.7 MeV. Evaluating the effect of this shift in perturbation theory,[10] $\Delta(\text{B.E.})/_A = \frac{1}{2}\kappa \times 7.7$ MeV ~ 0.57 MeV, where κ is the excitation probability out of the unperturbed fermi sea and is roughly 0.15 for ^{40}Ca. This effect clearly gives extra attraction in BHF, since the magnitude of the energy denominator is decreased.

(ii) A second difference is that partial waves higher than $j=2$ are omitted from BHF but included in LDAHF. The resulting change may be estimated by using the shift obtained by adding the $j=3$ partial waves with oscillator intermediate states given in Table II of Ref. 2 and assuming that partial waves above $j=3$ contribute negligibly. Here, the $j=3$ partial waves contribute 0.21 MeV repulsion, which is also in the right direction.

(iii) Finally, LDAHF included the Coulomb potential by treating all nucleons as having effective charge $\frac{1}{2}$ using Eq. (3.92) of Ref. 3 which yielded the proper direct Coulomb contribution but omitted one-half of the exchange Coulomb contribution. Adding one-half of the exchange energy which is roughly 6.3 MeV[11] increases the binding energy per particle by 0.08 MeV. Thus, the final result is that, accounting for these differences, BHF should be more bound by 0.86 MeV per particle which is in excellent agreement with the actual difference of 0.9 MeV. This precise agreement is partly fortuitous since quantitative corrections have not been made for two additional differences to be discussed subsequently. Nevertheless, it is a strong check on the validity of the LDA, and, in addition, on the accuracy of both calculations.

In order to compare density distributions from Refs. 1 and 2 with those of Ref. 3, several corrections must be applied. The technical differences (i)–(iii) which make BHF 0.9 MeV more bound than LDAHF also make the radius of BHF smaller relative to LDAHF and the interior density higher. From Figs. 3 and 4 of Ref. 2, one observes that small changes in the binding energy from shifting the spectrum or including $j=3$ partial waves simply scale the distributions: according to

$$\rho(r) \to \lambda^{-3}\rho\left(\frac{r}{\lambda}\right)$$

and λ may be obtained from the change in rms radius R, by $\lambda = 1 + \Delta R/R$. From Table II of Ref. 2, an increase of binding energy of 1.91 decreases the rms radius from 3.33 to 3.16 so that a change of 0.9 MeV yields $\Delta R/R = 0.0254$ or roughly a 7.5%

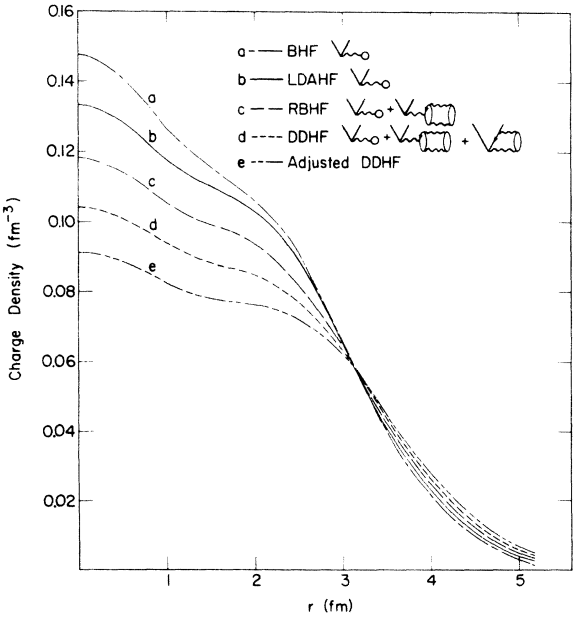

FIG. 2. Charge density distributions for ^{40}Ca as explained in the text.

change in central density. Since Fig. 4 of Ref. 3 contains charge distributions rather than point proton distributions, the densities of Refs. 1 and 2 must be folded with the proton charge distribution and corrected for center of mass motion as in Ref. 3. Although no ^{40}Ca BHF density with QTQ is plotted in Ref. 1 or 2, one observes that the QTQ RBHF density of Fig. 3 of Ref. 2 is undistinguishable from the oscillator RBHF with a shifted spectrum of Fig. 4 of Ref. 1. Thus, assuming that the difference between QTQ and the same shifted spectrum will also be negligible in the BHF case, we have scaled the unrenormalized curve of Fig. 4 of Ref. 1 by 2.54%, corrected for the proton size and c.m. correction and plotted this as the BHF curve a on our Fig. 2. This then should represent the result of a QTQ calculation corrected for the technical differences (i)–(iii) above.

Several comments concerning the discrepancy between the BHF and LDAHF densities of Fig. 2 are relevant. The discrepancy is most severe near the origin, where the r^2 phase space weighing is very small, and diminishes significantly beyond 1 fm. Also, the sign of the discrepancy may be easily understood on the basis of the two additional differences in the calculation (iv) and (v) for which we were unable to make explicit quantitative corrections as above for (i)–(iii).

(iv) The Pauli operator used in the QTQ calculation was a pure oscillator Q corresponding to $\hbar\Omega = 12.5$ MeV. The charge density corresponding to $\hbar\Omega = 12.5$ MeV is close to curve c of Fig. 2 and thus although Q is roughly self-consistent with the RBHF density, it is inconsistent with the BHF density. Clearly in the interior, this Q excludes too little phase space, making the G slightly too attractive, whereas in the surface, G becomes slightly too repulsive. Both effects tend to make the density too large in the interior and too small in the surface.

(v) There is a second small effect in the same direction arising from the parametrization of the LDA effective interaction below Eq. (2.26) of Ref. 3. The parametrization was designed to yield an optimum fit for densities less than or equal to $k_F = 1.4$ fm^{-1}, which is slightly beyond nuclear matter density and corresponds to a proton density of 0.093 fm^{-3}. As the density increases from $k_F = 1.0$ to 1.4 fm^{-1}, the $^3S_1$ attraction decreases rapidly, due to the Pauli operator blocking second order tensor correlations. Beyond $k_F = 1.4$ fm^{-1}, this decrease becomes much less rapid, as seen for example in Table I of Ref. 12 so that the parametrization optimized at lower densities becomes too repulsive at high densities. This additional repulsion tends to push curve b below curve a in Fig. 2, since the interior has attained an unphysically high density, but is, of course, irrelevant in physically sensible solutions which do not exceed $k_F = 1.4$ fm^{-1}. Although these two effects tend to reconcile the density difference in the two calculations, they will make the agreement in binding energies slightly worse. Corrections for both effects will be in the direction of increasing the LDAHF binding energy relative to the BHF energy, but since the 0.9 MeV discrepancy is already roughly accounted for, the additional corrections will likely make LDAHF slightly overbound relative to BHF.

It is desirable to eliminate the effect of the differences between the BHF and LDAHF distributions on subsequent comparisons. The RBHF curve in Fig. 2 is therefore not taken from Ref. 2, but has been obtained by multiplying the LDAHF density by the ratio of the renormalized RBHF and unrenormalized BHF densities in Fig. 4 of Ref. 1. This procedure assumes that the fractional change due to including occupation probabilities is the same in the LDAHF calculation as in the BHF calculation. It is intended to yield a RBHF density, curve c, which is free from the original differences between BHF and LDAHF and is then readily comparable with curves b, d, and e of Fig. 2 taken directly from Fig. 4 of Ref. 3.

III. CONCLUSIONS

From the agreement of curves a and b of Fig. 2 and the binding energies of BHF and LDAHF, we conclude that the technical differences in the calculation have been adequately accounted for and that the LDA is an excellent approximation as expected.

Having rendered the results of Refs. 1–3 comparable, Fig. 2 clearly displays the role of various mechanisms in producing saturation. Simply including diagram (a) of Fig. 1 with the unadjusted G matrix yields an interior density, curve b of Fig. 2, which is 45% too high compared with curve e which fits elastic electron scattering data,[13] or correspondingly an rms radius which is 15% too small. Inclusion of diagram (b) of Fig. 1 decreases the interior density, curve c of Fig. 2, by roughly 15%; diagram (c) of Fig. 1 decreases the density further by another 15%, curve d of Fig. 2; and finally the phenomenological parametrization of higher order corrections reduces the density by yet another 15% and yields excellent agreement with elastic electron scattering,[13] curve e of Fig. 2. Thus, each of the three terms is roughly comparable in its contribution to saturation.

Since the advent of DDHF calculations, a number of microscopic calculations have been carried out which include diagram (c) either explicitly[14,15] or implicitly through the use of a variational princi-

ple,[8,16,17] and all of these calculations indicate that this Pauli diagram (c) significantly improves saturation.

Within the framework of perturbation theory with the Tabakin interaction, Strayer[14] showed that diagrams (b) and (c) contribute roughly equally to the charge density of ^{40}Ca, as well as ^{16}O and ^{56}Ni. The leading correction terms in the diagramatic expansion for the one-body density operator are shown in diagrams (d) through (g) of Fig. 1, using the notation of Thouless.[18] Strayer showed that the contributions of diagrams (f) and (g) were each of the order of $\kappa\rho$, where in this calculation κ is the second-order contribution to the wound integral, 8% for ^{40}Ca, and ρ is the HF density. Diagram (d) is automatically summed by the self-consistent HF choice of the single-particle potential in Ref. 14.

Although diagram (e) was not explicitly calculated, it may be shown to be of the order of $\kappa\rho$, and thus comparable to diagram (f), by the following argument: The single-particle HF potential is reduced by a factor $1-\kappa$ when it is renormalized for occupation probabilities; that is, the contribution of the insertion in diagram (e) to the single-particle potential is approximately given by the insertion in diagram (h). The interior density will be changed by roughly the same fractional amount as the potential, as seen for example by a Thomas-Fermi argument. Thus, diagrams (e) and (f) yield density corrections of comparable magnitude, that is, of order $\kappa\rho$, and they correspond to the lowest order terms included in the diagrams (b) and (c). Diagram (g), of course, corresponds to the second order ladder included in our diagram (a), and the results of Ref. 14 are therefore consistent with our findings.

In Ref. 15, diagrams (b) and (c), as well as their hole-hole counterparts, were explicitly included in a calculation of ^{16}O using a second order approximation to the G matrix with plane wave intermediate states for the Sprung-de-Tourreil soft core interaction. Diagram (b) decreases the interior density by roughly 5% which, by the preceding argument, is expected from the fact that κ in this calculation is 5%. Diagram (c) decreases the interior density by approximately 10%, and given the crudeness of the G matrix and the extremely soft core of the interaction, these results are consistent with our conclusion that the contributions of diagrams (b) and (c) are comparable. The fact that the renormalization diagram (b) and the Pauli diagram (c) yield comparable contributions to the single-particle potential and the charge density was not recognized in the early theoretical discussions[6] and appears in the present context to be an important aspect of nuclear saturation.

The final 15% correction arising from the phenomenological parametrization of higher order diagrams is certainly not presently understood from fundamental principles. Nevertheless, we believe that it is significant that it is responsible for only about one-third of the difference in density between lowest order BHF theory and experiment and that two-thirds of the discrepancy may be accounted for by the contributions of diagrams (b) and (c) of Fig. 1.

---

*Research sponsored by the U. S. Atomic Energy Commission under contracts with the University of California, the Union Carbide Corporation, and the Massachusetts Institute of Technology.

†Permanent address: Physics Division, Oak Ridge National Laboratory, Oak Ridge, Tennessee 37830.

‡Alfred P. Sloan Foundation Research Fellow.

§Permanent address: Fakultät für Physik der Universität, 78 Freiburg/Breisgau, Germany.

[1]K. T. R. Davies and R. J. McCarthy, Phys. Rev. C 4, 81 (1971).

[2]K. T. R. Davies, R. J. McCarthy, and P. U. Sauer, Phys. Rev. C 6, 1461 (1972).

[3]J. W. Negele, Phys. Rev. C 1, 1260 (1970).

[4]J. W. Negele and D. Vautherin, Phys. Rev. C 5, 1472 (1972).

[5]M. W. Kirson, Nucl. Phys. A115, 49 (1968).

[6]B. H. Brandow, Ann. Phys. (N. Y.) 57, 214 (1970).

[7]L. Schäfer and H. A. Weidenmüller, Nucl. Phys. A215, 493 (1973).

[8]S. Coon, University of Arizona (to be published).

[9]X. Campi and D. W. L. Sprung, Nucl. Phys. A194, 401 (1972).

[10]H. A. Bethe, Annu. Rev. Nucl. Sci. 21, 93 (1971).

[11]A. E. S. Green, Phys. Rev. 112, 1719 (1958).

[12]H. A. Bethe, Phys. Rev. 167, 879 (1968).

[13]J. W. Negele, Phys. Rev. Lett. 27, 1291 (1971).

[14]M. R. Strayer, MIT Ph.D. thesis (unpublished); M. R. Strayer, W. H. Bassichis, and A. K. Kerman, Phys. Rev. C 8, 1269 (1973).

[15]B. Rouben, R. Padjen, and G. Saunier, to be published.

[16]R. K. Tripathi, A. Faessler, and A. D. MacKellar, Phys. Rev. C 8, 129 (1973).

[17]S. Y. Rao, Ph.D. thesis, University of Maryland, 1972 (unpublished).

[18]D. J. Thouless, *The Quantum Mechanics of Many Body Systems* (Academic, New York, 1961).